The first quantitative estimation of the influence of volcanic activity on noctilucent clouds

Peter Dalin[1,2 *], Nikolay Pertsev[3], Vladimir Perminov[3], & Vitaly Romejko[4]

[1] Swedish Institute of Space Physics, Box 812, SE-981 28 Kiruna, Sweden

[2] Space Research Institute, RAS, Profsouznaya st. 84/32, Moscow, 117997, Russia

[3] A.M. Obukhov Institute of Atmospheric Physics, RAS, Pyzhevskiy per. 3, Moscow, 119017, Russia

[4] The Moscow Association for NLC Research, Kosygina st. 17, Moscow, 119334, Russia

*Corresponding author at: Swedish Institute of Space Physics, Box 812, SE-981 28 Kiruna, Sweden. Fax: +46 980 79050. E-mail address: pdalin@irf.se (P. Dalin).

Abstract

Climate change happening in the middle and upper atmosphere has been intensively investigating nowadays. One of the experimental tools to investigate long-term changes in the mesopause region between 80 and 90 km altitude is a natural atmospheric phenomenon called noctilucent clouds (NLCs). Being composed of tiny ice particles, NLCs are supposed to be highly sensitive to small changes in the temperature and amount of water vapor at the polar summer mesopause. Many factors such as solar activity, long-term changes in the temperature, amount of water vapor, minor atmospheric constituents, have been considered contributing to long-term NLC changes. At the same time, a role of volcanic activity in the NLC variability has been investigated in a qualitative sense in previous studies so far, and its influence has been found to be inconclusive. For the first time, we quantitatively investigate a factor of volcanic activity in NLC variability for the past five decades. Our analysis reveals that there is statistically significant positive influence of volcanic activity on changes in NLC activity, with a time lag of 7 years between these processes which might be explained by a slow meridional-vertical updraft of ejected volcanic water vapor from the tropical troposphere to the polar mesopause region. We confirm our previous

results on no statistically significant long-term trend in NLC activity at middle and subpolar latitudes for the past five decades.

1. Introduction

Spectacular night-shining clouds or noctilucent clouds (NLCs) are the highest clouds in the Earth's atmosphere observed at the summer mesopause between 80 and 90 km. NLCs can be readily seen from mid- and subpolar latitudes of both hemispheres. NLCs are composed of water-ice particles of 30–100 nm in radius that scatter sunlight and thus NLCs are observed against the dark twilight arc from May until September in the Northern Hemisphere and from November to February in the Southern Hemisphere (Bronshten & Grishin, 1970; Gadsden & Schröder, 1989). NLCs are also observed from space and in this case they are usually called Polar Mesospheric Clouds, PMCs (Thomas, 1984).

A small size of NLC ice particles makes them a perfect natural indicator of potential climate change happening in the middle atmosphere. For comparison purposes note that ice particles of cirrus tropospheric clouds are by one-four orders of magnitude greater than NLC ice crystals (Kärcher et al., 2014). Since 1990s, there is a growing interest in studies of long-term time series of NLCs/PMCs (Berger & Lübken, 2015; Dalin et al., 2006, 2020; DeLand et al., 2006, 2015, 2019; Dubietis et al., 2010; Fiedler et al., 2017; Gadsden, 1990, 1997; Hervig & Siskind, 2006; Kirkwood et al., 2003, 2008; Lübken & Berger, 2011; Lübken et al., 2018; Pertsev et al., 2014; Romejko et al., 2003; Shettle et al., 2009; Zalcik et al., 2016). Up to now, various methods (model simulations, ground-based NLC observations, PMC measurements from space) show various results on long-term trends in NLC/PMC activity, which demonstrate the complexity of the problem (Dalin et al., 2020). However, in order to retrieve correct information on long-term changes in NLCs one needs to separate their long-term changes in time from other solar-geophysical processes having interannual and decadal variabilities. Thus, the 11-year solar cycle, interannual and long-term variations in the content of water vapor, ozone, carbon dioxide and methane have been considered in a wealth of papers dealing with long-term trends in NLCs/PMCs (Berger & Lübken, 2015; Dalin et al., 2020; DeLand et al., 2015, 2019; Fiedler et al., 2017; Hervig & Siskind, 2006; Lübken & Berger, 2011; Lübken et al., 2018; Pertsev et al., 2014). However, a volcanic factor as a driver of variability in the NLC activity has been scantly addressed so far, mainly by

qualitatively considering major volcanic eruptions only (Bronshten & Grishin, 1970; Gadsden & Schröder, 1989; Fogle & Haurwitz, 1973; Hervig et al., 2016; Thomas & Olivero, 2001; Thomas et al., 1989). It has been found that after some major eruptions (Krakatoa in 1883, Bezymianny in 1956, Agung in 1963) there was an increase in NLC activity whereas other volcanic events (Okataina in 1886, Mount Pelée and Santa Maria in 1902, Tarumai in 1909, Taal in 1911, Katmai in 1912) did not result in increased NLC activity (Bronshten & Grishin, 1970; Dalin et al., 2012; Fogle & Haurwitz, 1973; Gadsden & Schröder, 1989; Thomas & Olivero, 2001). In general, conflicting evidences of the influence of volcanic activity on NLC activity have been obtained (Fogle & Haurwitz, 1973). In a recently published paper (Lübken et al., 2018) dealing with model studies of long-term trends in NLCs, the authors have noted that the role of volcanic eruptions for long-term evolution of NLCs should be addressed in more detail. This motivated us to reinvestigate a volcanic factor as a potential driver for long-term evolution of NLCs based, for the first time, on high quality long-term data series of NLC and volcanic activities as well as using a robust statistical method of the present analysis.

2. Data Source

Long-term data series of NLC observations conducted in the Moscow region in Russia (~56°N, 37°E) for the period of 1968-2018 have been used. The full Moscow NLC database analyzed in the present paper is available at the project website: http://ifaran.ru/lab/lfva/NLC_data_engl.html. We utilize two parameters characterizing yearly NLC activity: the NLC occurrence number and NLC brightness. The full description of the NLC database, method of observations and estimated parameters can be found in Romejko et al. (2003) and Dalin et al. (2020).

Time series of the Lyman α flux at 121.6 nm as a proxy of solar activity have been utilized for the period of 1968-2018, which were obtained from the LASP Interactive Solar Irradiance Datacenter (LISIRD) available at http://lasp.colorado.edu/lisird.

We have used quantitative information on global volcanic activity for the past five decades available at the Global Volcanism Program of the Smithsonian Institute (http://volcano.si.edu/search_eruption.cfm#.). Volcanic eruptions are classified by the Volcanic Explosivity Index (VEI) that describes the magnitude of an explosive volcanic eruption. The VEI scale extends from 0 to 8 marks, representing a logarithmic scale in which an increase of 1 unit corresponds to an increase of intensity

of a factor of 10. VEI includes the following eruption characteristics: total volume of explosive products, height of eruptive cloud above the vent, eruption type, duration of continuous blast, extent of tropospheric and stratospheric injection and some other descriptive characteristics (Newhall & Self, 1982; Siebert et al., 2010).

Since several tens of volcanic eruptions occur each year, we have made the following processing of the VEI value in order to make it comparable to yearly numbers of the NLC activity:

a) each volcanic year has been defined from May to May of two successive calendar years. This is due to the fact NLCs start to be visible from late May at middle latitudes.

b) the sum of all VEI values has been calculated for each volcanic year, i.e., we define and analyze the total (accumulated) VEI value for each volcanic year. This is because one can expect a cumulative volcanic influence on NLCs in term of a cumulative injection of water vapor, methane and fine dust for each volcanic year.

3. Method of Analysis

Multiple regression analysis (MRA) has been applied to the analyzed NLC parameters:

$$Y = C_0 + C_1 \cdot (t - 1968) + C_2 \cdot F_{Lya}(t - t_{lag2}) + C_3 \cdot VEI(t - t_{lag3}) \quad (1)$$

where Y is the yearly estimated NLC parameter (either the NLC occurrence number or NLC brightness), C_0 is the regression constant, C_1, C_2 and C_3 are the regression coefficients characterizing the linear long-term trend (Value per year, V/yr), solar activity term (Value per SFU, solar Ly-α flux units, 1 SFU is 10^{11} photons $s^{-1}cm^{-2}$) and volcanic activity term (Value per VEI value); t_{lag2} and t_{lag3} are the phase time lags between the NLC parameter and solar activity and volcanic activity, respectively, F_{Lya} is the Lyman α flux averaged over each summer season (June-July), and VEI is the total (accumulated) volcanic explosivity index for each volcanic year. The same MRA technique has been frequently utilized in geophysical data analysis (Dalin et al., 2020; DeLand et al., 2015; Dubietis et al., 2010; Kirkwood et al., 2008; Pertsev et al., 2014).

All statistical errors presented in the paper have been calculated using the least-squares method (Jenkins & Watts, 1968). The number of observations (N value) is

equal to 51 for NLC, volcanic and solar time series. The degree of freedom is 47. We calculate various statistical significance levels (either 90% ~ 1.5σ, or 95% ~ 2σ, or 99% ~ 3σ) for the estimated regression coefficients (C_0, C_1, C_2 and C_3) in order to demonstrate as high statistical significance for a particular regression coefficient as possible. The P values for the null hypothesis test have been calculated for each regression coefficient as well. All statistical levels as well as P values are presented in Table 1.

4. Results

4.1. Overview of the analyzed data on volcanic activity and noctilucent clouds.

The analyzed data on volcanic and NLC activity for the period of 1968-2018 are shown in Fig. 1. In this research, we analyze volcanic activity represented by VEI values on a logarithmic scale (not on a linear scale). The reason for this is as follows. We assume that the main driver of volcanic eruptions on NLC activity is due to erupted water vapor to the troposphere and stratosphere which slowly ascend to the mesopause region (80-90 km) as will be considered in the Discussion. Unfortunately, there are no available estimations of amounts and eruptive heights of injected water vapor to the atmosphere after each volcanic eruption so far. Fortunately, in the analyzed volcanic data base there are estimations of the mass and eruptive altitudes of one of the main volcanic gas sulfur dioxide (SO_2). These estimations were made based on satellite measurements for some small part of volcanic eruptions, i.e., for about 15% of all analyzed volcanic eruptions for the past five decades. The eruptive altitudes and masses of SO_2 as a function of VEI values are shown in Fig. 2 (panels a and b, respectively). One can see that there are wide ranges of SO_2 altitudes and masses for a given VEI value (black dots), that is especially valid for small and moderate eruptions with VEI values from 1 to 3. At the same time, we can estimate mean values of the altitudes and masses of SO_2 for each VEI value, which are shown in Fig. 2 by red dots. A statistical F-test demonstrates that the mean values are well described by the logarithmic function of VEI values (the blue lines in Fig. 2a and Fig. 2b have 96% and 88% significance, respectively). Since water vapor is one of the main volcanic gases (Symonds et al., 1994), we can assume that masses and altitudes of eruptive water vapor have the logarithmic dependence of VEI values as well. Further we will consider NLC activity as a function of the sum of VEI values for each year for the period of 1968-2018.

4.2. Dependence of noctilucent cloud activity on volcanic activity.

Since the phase time lag between NLC and volcanic activities (t_{lag3}) is completely unknown so far, we have performed our analysis using t_{lag3} values in a wide range from minus ten to plus ten years. The minus/ plus phase shift means that NLC activity is ahead of/ follows volcanic one. All the calculated regression coefficients and time lags of equation (1) are summarized in Table 1.

The calculated volcanic regression coefficient C_3 as a function of the time lag is illustrated in Fig. 3a,c. We can see there is statistically significant (90%) positive volcanic regression coefficient C_3 with the correlation lag equal to +7 years in the case of the NLC occurrence number (Fig. 3a). The cross-correlation coefficient for this peak value is +0.35 (Fig. 3b). At the same time, the cross-correlation coefficient between NLC and solar activity is equal to –0.30 with the phase lag of zero years, i.e., less than the cross-correlation coefficient of volcanic activity. This finding clearly illustrates a comparable and even dominating role of the volcanic forcing relative to well-known anticorrelation solar influence leading to photodissociation of water molecules at the mesopause region. The same analysis has been performed for the NLC brightness. Figure 3c demonstrates us that there is statistically significant (90%) positive influence of volcanic activity on the NLC brightness, with the same +7 years phase shift as obtained for the NLC occurrence number. The cross-correlation coefficient of this peak regression value is equal to +0.36 (Fig. 3d), again slightly greater by absolute value than the cross-correlation coefficient of solar activity.

Now we consider the influence of volcanic activity on NLCs by selecting volcanic eruptions which occurred at equatorial and subtropical latitudes between 30°S and 30°N. The reason for this is considered in the Discussion. One can see that for the NLC occurrence number (Fig. 4a) the volcanic regression coefficient has now increased from 0.11 to 0.15 at the 7-year time lag, and its statistical significance has also become higher than 95%. A similar result has been obtained for the NLC brightness (Fig. 4c), which shows statistically significant (95%) positive influence of volcanic activity with the same phase shift of +7 years. The maximum cross-correlation coefficients for the NLC occurrence number and brightness are +0.39 (Fig. 4b,d), i.e., greater than in case when considering all volcanic eruptions that occurred around the world.

One can investigate a role of the power of volcanic eruptions influencing the NLC activity. We can do it by selecting volcanic eruptions in accordance to their VEI values. As in Fig. 4, all the eruptions have been considered in the latitude band between 30°S and 30°N. The volcanic regression coefficients for minor volcanic eruptions, having VEI values equal to 1 and 2 points, are shown for the NLC occurrence number (Fig. 5a) and NLC brightness (Fig. 5c). One can see none of volcanic regression coefficients (C_3) are statistically significant. At the same time, if we consider moderate and large volcanic eruptions with VEI values equal to 3 points and more, then the picture dramatically changes: highly statistically significant volcanic influence (99%) is found for both the NLC occurrence number (Fig. 5b) and NLC brightness (Fig. 5d), with the same phase lag equal to +7 years. Note that such a high statistical significance of 99% in the NLC occurrence number and brightness is rarely observed in actual geophysical data having large random errors due to the presence of various processes. Nevertheless, the 99% statistical significance of the volcanic driver on NLC activity does exist in the analyzed data sets.

5. Discussion

About zero long-term trend in the occurrence frequency of noctilucent clouds and small positive statistically insignificant long-term trend in their brightness (see coefficients C_1 in Table 1) have been obtained in the present study. It means that these small trends are not reliable and they might readily change their signs in the years to come. This result agrees with numerous ground-based NLC observations performed around the world (Dalin et al., 2006, 2020; Dubietis et al., 2010; Kirkwood & Stebel, 2003; Kirkwood et al., 2008; Pertsev et al., 2014; Romejko et al, 2003; Zalcik et al., 2016), which clearly demonstrated about zero and/or small positive statistically insignificant trends in NLC occurrence number and brightness for the past five decades.

The reason for the selection of volcanic eruption in relation to latitudes is as follows. In the equatorial troposphere, there is an overturning wind circulation called the Hadley Cells, in which the warm air rising at the equator sinks at around 30°S and 30°N latitudes where the Hadley Cells end (Brasseur & Solomon, 1986). However, the Hadley Cells are not completely closed circulations. Part of the air penetrates into the stratosphere in the tropics, then traveling towards polar latitudes of the summer hemisphere, where it again rises to the summer mesosphere, and finally reaches the

summer mesopause (Brasseur & Solomon, 1986; Garcia & Solomon, 1983). This meridional-vertical air circulation is supposed to be one of the main sources of water vapor at the mesopause region to form NLC ice particles (Thomas, 1991). Another important source of water vapor in the mesosphere is due to methane oxidation (Brasseur & Solomon, 1986; Thomas, 1991). The photochemical lifetime of methane in the troposphere, stratosphere and lower mesosphere is long enough (several years) to produce sufficient amount of water vapor in the mesosphere and mesopause, i.e., one methane molecule produces about two molecules of water vapor (Thomas, 1991). Our finding supports the penetration of volcanic gases (water vapor and methane) from the troposphere through the tropical upwelling to the polar mesopause region by highly statistically significant positive influence of volcanic activity on NLCs when considering volcanic eruptions that occurred at the subtropics between 30°S and 30°N. Higher volcanic activity leads to higher positive influence on NLC activity that is explained by larger amounts of volcanic gases injected to the tropical troposphere and lower stratosphere, including water vapor and methane.

The found 7 years phase lag between volcanic and NLC activity is supported by experimental studies dealing with the transport time of minor atmospheric species from the troposphere to the stratosphere and mesosphere. Thus, the transport time of inert trace gases (N_2O, CF2C12, CFC13 and CC14) from the ground to the stratosphere (at 20-30 km altitude) have been observed to be of the order of 3-4 years (Stordal et al., 1985). Russell III *et al*. (1996) have found that the transport time of hydrogen fluoride (HF) trace gas is 5.9±2 years to be lifted from the lower troposphere to the mesosphere at 55 km altitude. The transport time of the CO_2 trace gas (as measured in a balloon-borne experiment) was found to be about 5 years to reach the polar stratosphere at 35 km altitude from the troposphere through the tropical upwelling (Bischof et al., 1985). Thus, it takes about 4-6 years for inert trace gases to reach the polar atmosphere at 30-55 km altitude from the tropical troposphere. Then it takes them two years more to rise throughout the mesosphere and reaching the mesopause region at 85-87 km altitude where NLC ice particles start to form. The latter is supported by a well know fact that first undoubtedly detected NLCs were discovered in June 1885, i.e., about two years after the explosive Krakatoa eruption occurred in August 1883. Note that the most likely altitude of the Krakatoa eruption column was about 40–50 km (Carey & Sparks, 1986; Self & Rampino,

1981). As a result, the total time required transporting volcanic water vapor and methane from the tropical troposphere to the polar mesopause is about 6-8 years. This does not apply to the most violent volcanic eruptions, such as Krakatoa, El Chichón and Pinatubo, in which volcanic plumes can be injected higher up into the middle and upper stratosphere. Our finding of the 7 years time delay between NLCs and volcanic activity is in a good agreement with the above mentioned experimental estimations.

Another potential volcanic mechanism influencing NLC activity is as follows. Besides water vapor and methane, volcanic eruptions inject SO_2 into the stratosphere, which leads to increased sulfate aerosol optical depth, which in turn warms the stratosphere (Randel et al., 2009). Warming of the stratosphere results in warming of the mesosphere and mesopause through hydrostatic atmospheric expansion (Akmaev et al., 2006), which in turn should lead to a decrease in NLC activity, i.e., one can anticipate an anticorrelation behavior between volcanoes and NLCs in this case. However, by looking at the volcanic regression coefficient (C_3) as a function of time lag shown in Figs. 3-5, we see that all negative volcanic regression coefficients are less compared to the pronounced positive volcanic regression coefficient at the lag of 7 years, and all these negative volcanic regression coefficients have small or no statistical significance at all. This does not necessarily exclude the presence of the volcanic warming mechanism but compared to the injection and transport of water vapor, the latter seems to play a more significant role in establishing the connection between NLCs and volcanic activity.

The limitations of our statistical study are due to unknown amounts of injected volcanic water vapor after each eruption, how much ejected water vapor are actually transported through the stratosphere and mesosphere as well as how long does it actually take to transport volcanic gases to mesopause heights after each eruption. This task is complicated. Indeed, a model study by Pinto et al., 1989 has clearly indicated that after major volcanic eruptions increased water vapor in the stratosphere is limited by condensation in the rising volcanic plume and stabilized ash cloud (cold trap effect). The authors have emphasized that "*Cold trap effects in volcanic eruption columns could exert significant controls on the amounts of water vapor and halogens that remain in stratospheric volcanic clouds, through condensation on ash particles followed by the fallout of the particles. It is extremely difficult to estimate the amount of HCI and H_20 remaining in the stratosphere after volcanic eruptions, based on current data and modeling capabilities*." At the same time, the results of our statistical

study (positive response of NLCs to volcanic activity with a 7 years phase lag) are consistent with a general atmospheric meridional-vertical circulation of minor atmospheric species from the tropical troposphere to the polar mesopause region. This will further stimulate us to make a sophisticated research dealing with satellite measurements of water vapors in relation to volcanic eruptions, estimating H_2O transport through the troposphere, stratosphere and mesosphere, and finding a robust link between erupted volcanic water vapor and activity of noctilucent clouds.

6. Conclusions

We have analyzed long-term data sets of noctilucent clouds, volcanic and solar activity from 1968 to 2018 and conclude the following:

1. For the first time, we have quantitatively investigated a factor of volcanic activity in variability of NLCs for the past five decades. Our analysis reveals that there is statistically significant positive influence of volcanic activity on changes in NLC activity, with a time lag of 7 years between these processes which might be explained by a slow meridional-vertical updraft of ejected volcanic water vapor from the tropical troposphere to the polar mesopause.
2. The strongest influence of volcanic activity on NLCs, with 99% statistical significance, is found for volcanic eruptions that occurred at tropical latitudes between 30°S and 30°N, with VEI values equal and more than 3.
3. We have confirmed our previous results on no statistically significant long-term trend in NLC activity at middle and subpolar latitudes for the past five decades as well as statistically significant negative response of NLCs to solar activity.

Acknowledgements: The authors are grateful to all amateur observers for their help in visual observations of noctilucent clouds conducted in the Moscow region from 1962 to 2002. The work was partly supported by the Russian Foundation for Basic Research under project 19-05-00358a. The analyzed data sets on noctilucent clouds, solar and volcanic activity (on a yearly base) for the period of 1968-2018 is available at the project web site:
http://ifaran.ru/lab/lfva/terrestrial_and_space_effects_in_NLC.html?&locale=en

References

Akmaev, R. A., Fomichev, V. I. & Zhu, X. (2006). Impact of middle-atmospheric composition changes on greenhouse cooling in the upper atmosphere. *Journal of Atmospheric and Solar-Terrestrial Physics*, 68, 1879–1889.

Berger, U. & Lübken, F.-J. (2015). Trends in mesospheric ice layers in the Northern Hemisphere during 1961–2013. *Journal of Geophysical Research-Atmospheres*, 120, 11277–11298.

Bischof, W., Borchers, R., Fabian, P. & Krüger, B. C. (1985). Increased concentration and vertical distribution of carbon dioxide in the stratosphere. *Nature*, 316, 708-710.

Brasseur, G. & Solomon, S. (1986). *Aeronomy of the middle atmosphere.* Second Edition, D. Reidel Publishing Company, Dordrecht, Holland.

Bronshten, V. A., & Grishin, N. I. (1970). *Noctilucent clouds.* Nauka, Moscow.

Carey, S. N. & Sparks, R. S. J. (1986). Quantitative models of fallout and dispersal of tephra from volcanic eruption columns. *Bulletin of Volcanology*, 48, 109–125.

Dalin, P., Kirkwood, S., Andersen, H., Hansen, O., Pertsev, N., Romejko, V. (2006). Comparison of long-term Moscow and Danish NLC observations: statistical results. *Annales Geophysicae*, 24, 2841-2849.

Dalin, P., Pertsev, N. & Romejko, V. (2012). Notes on historical aspects on the earliest known observations of noctilucent clouds. *History of Geo- and Space Sciences*, 3, 87–97.

Dalin, P., Perminov, V., Pertsev, N. & Romejko, V. (2020). Updated long-term trends in mesopause temperature, airglow emissions, and noctilucent clouds. *Journal of Geophysical Research-Atmospheres*, 125, e2019JD030814, https://doi.org/10.1029/2019JD030814.

DeLand, M. T., Shettle, E. P., Thomas, G. E. & Olivero, J. J. (2006). A quarter-century of satellite PMC observations. *Journal of Atmospheric and Solar-Terrestrial Physics*, 68, 9–29.

DeLand, M. T., & Thomas, G. E. (2015). Updated PMC trends derived from SBUV data. *Journal of Geophysical Research-Atmospheres*, 120, 2140-2166.

DeLand, M. T. & Thomas, G. E. (2019). Extending the SBUV polar mesospheric cloud data record with the OMPS NP. *Atmospheric Chemistry and Physics*, 19, 7913–7925.

Dubietis, A., Dalin, P., Balciunas, R. & Cernis, K. (2010). Observations of noctilucent clouds from Lithuania. *Journal of Atmospheric and Solar-Terrestrial Physics*, 72, 14-15, 1090-1099.

Etiope, G. & Milkov, A. V. (2004). A new estimate of global methane flux from onshore and shallow submarine mud volcanoes to the atmosphere. *Environmental Geology*, 46, 997-1002.

Fiedler, J., Baumgarten, G., Berger, U. & Lübken, F.-J. (2017). Long-term variations of noctilucent clouds at ALOMAR. *Journal of Atmospheric and Solar-Terrestrial Physics*, 162, 79–89.

Fogle, B. & Haurwitz, B. (1973). Long term variations in Noctilucent cloud activity and their possible cause. *Climatological Research*, 263–276, Bonner Meteorologische Abhandlungen, Bonn, Germany.

Gadsden, M. (1997). The secular changes in noctilucent cloud occurrence: Study of a 31-year sequence to clarify the causes. *Advances in Space Research*, 20(11), 2097–2100.

Gadsden, M. (1990). A secular change in noctilucent cloud occurrence. *Journal of Atmospheric and Terrestrial Physics*, 52(4), 247-251.

Garcia, R. R. & Solomon, S. (1983). A numerical model of the zonally averaged dynamical and chemical structure of the middle atmosphere. *Journal of Geophysical Research*, 88(C2), 1379-1400.

Hervig, M. & Siskind, D. (2006). Decadal and inter-hemispheric variability in polar mesospheric clouds, water vapor, and temperature. *Journal of Atmospheric and Solar-Terrestrial Physics*, 68, 30–41.

Hervig, M. E., Berger, U. & Siskind, D. E. (2016). Decadal variability in PMCs and implications for changing temperature and water vapor in the upper mesosphere. *Journal of Geophysical Research-Atmospheres*, 121, 2383–2392.

Jenkins, G. M. & Watts, D. G. (1968). *Spectral analysis and its applications*. Holden-Day, San Francisco.

Kirkwood, S. & Stebel, K. (2003). Influence of planetary waves on noctilucent cloud occurrence over NW Europe. *Journal of Geophysical Research*, 108(D8), 8440, doi: 10.1029/2002JD002356.

Kirkwood, S., Dalin, P. & Réchou, A. (2008). Noctilucent clouds observed from the UK and Denmark—Trends and variations over 43 years. *Annales Geophysicae,* 26, 1243–1254.

Kärcher, B., Dörnbrack, A. & Sölch, I. (2014). Supersaturation variability and cirrus ice crystal size distributions. *Journal of the Atmospheric Sciences*, 71, 2905-2926.

Lübken, F.-J. & Berger, U. (2011). Latitudinal and interhemispheric variation of stratospheric effects on mesospheric ice layer trends. *Journal of Geophysical Research,* 116, D00P03, doi:10.1029/2010JD015258.

Lübken, F.-J., Berger, U. & Baumgarten, G. (2018). On the anthropogenic impact on long-term evolution of noctilucent clouds. *Geophysical Research Letters,* 45, 6681–6689.

Newhall, C. G. & Self, S. (1982). The Volcanic Explosivity Index (VEI): an estimate of explosive magnitude for historical volcanism. *Journal of Geophysical Research,* 87, 1231–1238.

Pertsev, N., Dalin, P., Perminov, V., Romejko, V., Dubietis, A., Balčiunas, R. et al. (2014). Noctilucent clouds observed from the ground: sensitivity to mesospheric parameters and long-term time series. *Earth, Planets and Space,* 66(98), doi:10.1186/1880-5981-66-98.

Pinto, J. P., Turco, R. P. & Toon, O. B. (1989). Self-limiting physical and chemical effects in volcanic eruption clouds. *Journal of Geophysical Research,* 94(D8), 11165-11174.

Randel, W. J., Shine, K. P., Austin, J., Barnett, J., Claud, C., Gillett, N. P. *et al*. (2009). An update of observed stratospheric temperature trends. *Journal of Geophysical Research,* 114, D02107, doi:10.1029/2008JD010421.

Romejko, V. A., Dalin, P. A. & Pertsev, N. N. (2003). Forty years of noctilucent cloud observations near Moscow: database and simple statistics. *Journal of Geophysical Research,* 108(D8), 8443, doi:10.1029/2002JD002364.

Russell III, J. M., Luo, M., Cicerone, R. J. & Deaver, L. E. (1996). Satellite confirmation of the dominance of chlorofluorocarbons in the global stratospheric chlorine budget. *Nature,* 379, 526–529.

Self, S. & Rampino, M. (1981). The 1883 eruption of Krakatau. *Nature,* 294, 699–704.

435 Shettle, E. P., DeLand, M. T., Thomas, G. E. & Olivero, J. J. (2009). Long term
436 variations in the frequency of polar mesospheric clouds in the Northern Hemisphere
437 from SBUV. *Geophysical Research Letters*, 36, L02803, doi:10.1029/2008GL036048.
438 Siebert, L., Simkin, T. & Kimberly, P. (2010). *Volcanoes of the World.* Third
439 Edition, University of California Press, Los Angeles.
440 Sigurdsson, H., Carey, S., Mandeville, C. & Bronto, S. (1990). Krakatau volcano
441 expedition 1990. *Report to the National Geographic Society*, 37 pp..
442 Stordal, F., Isaksen, I. S. A. & Horntveth, K. (1985). A diabatic circulation two-
443 dimensional model with photochemistry: simulations of ozone and long-lived tracers
444 with surface sources. *Journal of Geophysical Research*, 90(D3), 5757-5776.
445 Symonds, R.B., Rose W. I., Bluth G. J. S., & Gerlach T. M. (1994). Volcanic gas
446 studies: methods, results, and applications, *Volatiles in Magmas: Reviews in*
447 *Mineralogy*. Mineralogical Society of America, Washington, D.C., Eds. Carroll, M.
448 R., & Holloway, J. R., 30. 1-66.
449 Thomas, G. E. (1984). Solar Mesosphere Explorer measurements of polar
450 mesospheric clouds (noctilucent clouds). *Journal of Atmospheric and Terrestrial*
451 *Physics*, 46(9), 819-824.
452 Thomas, G. E., Olivero, J. J., Jensen, E. J., Schroeder,W. & Toon, O. B. (1989).
453 Relation between increasing methane and the presence of ice clouds at the mesopause.
454 *Nature*, 338, 490–492.
455 Thomas, G. E. (1991). Mesospheric clouds and the physics of the mesopause
456 region. *Reviews of Geophysics*, 29(4), 553-575.
457 Thomas, G. E., and Olivero, J. (2001). Noctilucent clouds as possible indicators of
458 global changes in the mesosphere. *Advances in Space Research*, 28(7), 937-946.
459 Zalcik, M. S., Lohvinenko, T. W., Dalin, P. & Denig, W. F. (2016). North
460 American noctilucent cloud observations in 1964-77 and 1988-2014: analysis and
461 comparisons. *Journal of the Royal Astronomical Society of Canada*, 110(1), 8-15.
462

Figures

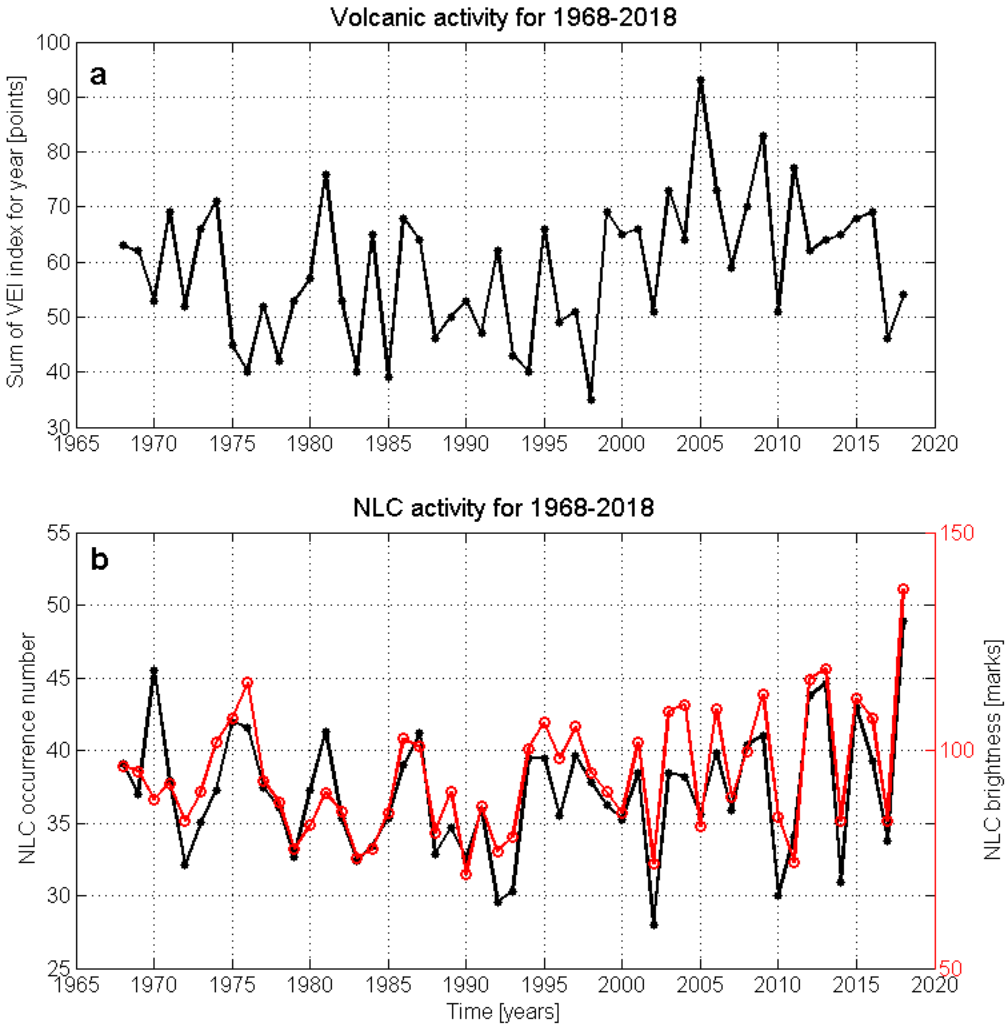

Figure 1. Overview of the analyzed data sets. **(a)** Volcanic activity data are represented by a sum of VEI values for each year from 1968 to 2018. Note that the two main eruptions in the time period considered (El Chichón in 1982 and Pinatubo in 1991) do not show up in the annually accumulated VEI values. **(b)** Annual NLC activity for the period of 1968-2018 is represented by the annual NLC occurrence number (black line with dots, left Y axis) and by the annual NLC brightness (red line with open circles, right Y axis).

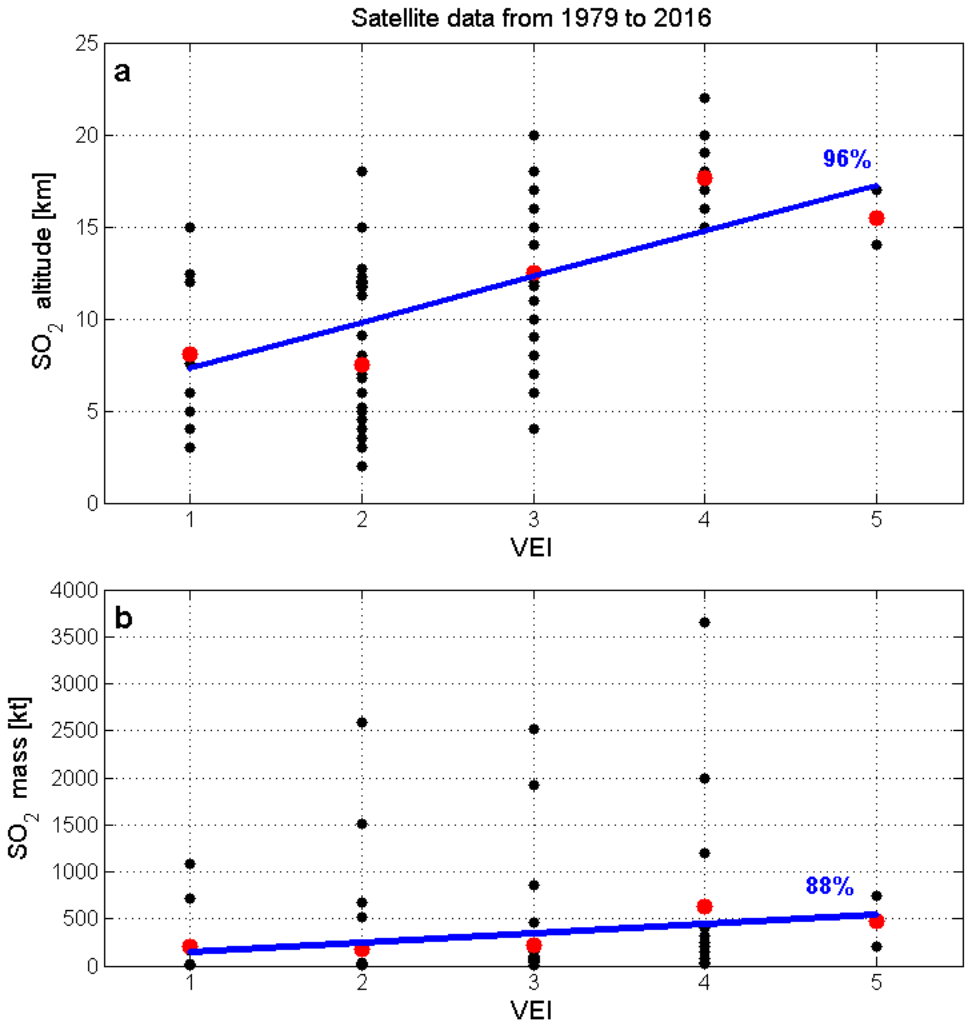

Figure 2. Satellite measurements of volcanic SO_2 emissions. **(a)** The black dots are eruptive altitudes of SO_2 emissions as a function of VEI values. The red dots are SO_2 mean altitudes for the respective VEI values. The blue line is a linear function of mean SO_2 altitudes fitted in the least-square sense. **(b)** Same as in **(a)** except for the mass of ejected SO_2 emissions. Note that the X axis represents a logarithmic scale of the volcanic activity (VEI values). Linear regression functions are statistically significant with probabilities of 96% **(a)** and 88% **(b)**.

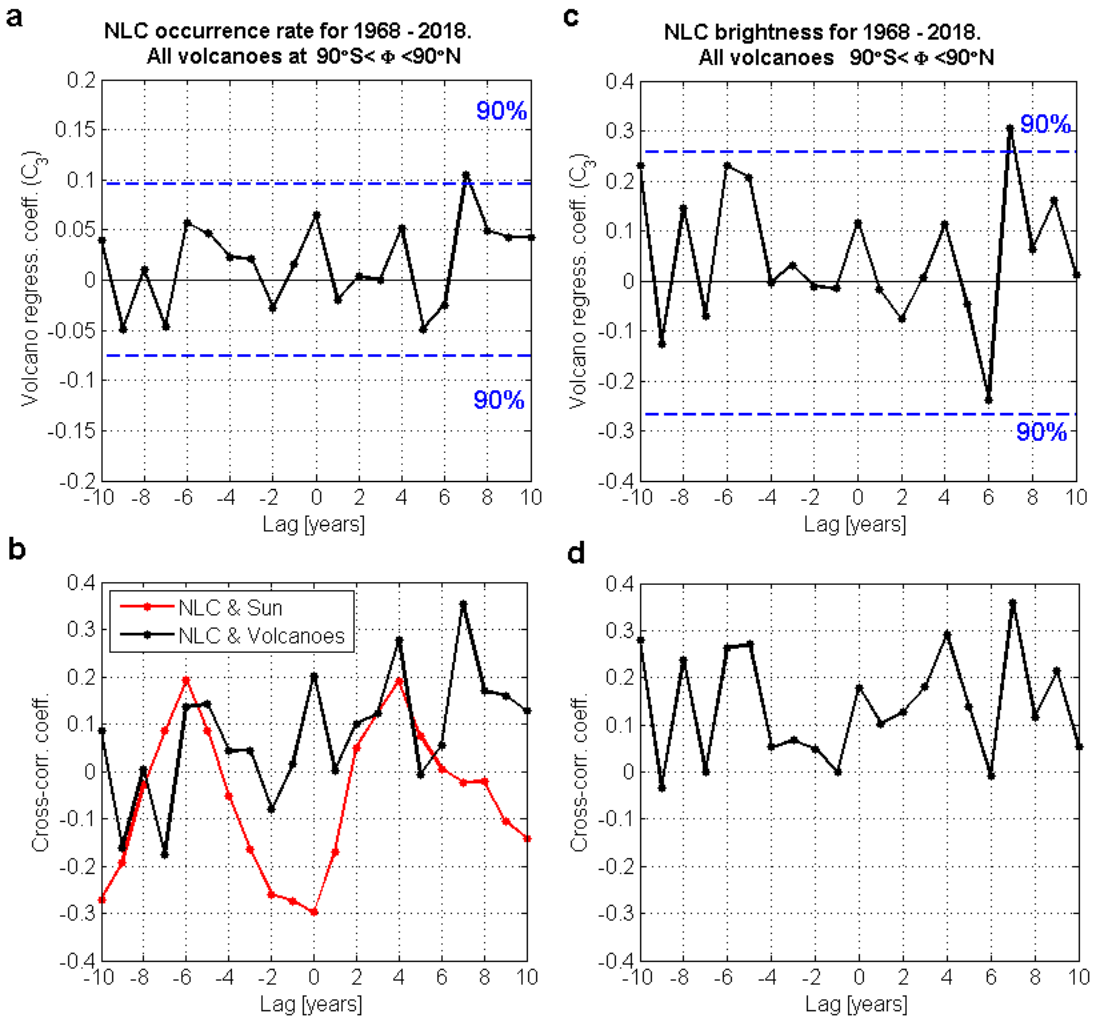

480

481 **Figure 3.** Statistical quantities characterizing a connection between volcanic and NLC
482 activity for all volcanic eruptions that occurred around the world. **(a)** The black line
483 shows the volcanic regression coefficient (C_3) as a function of the phase time lag for
484 the NLC occurrence number. The blue lines indicate 90% confidence intervals of the
485 maximum value of the C_3 coefficient. **(b)** The back line shows the cross-correlation
486 coefficient between the NLC occurrence number and volcanic activity. The red line
487 represents the cross-correlation coefficient between the NLC occurrence number and
488 solar Lyman α flux. **(c)** Same as in **(a)** except for the NLC brightness. **(d)** The black
489 line shows the cross-correlation coefficient between the NLC brightness and volcanic
490 activity.

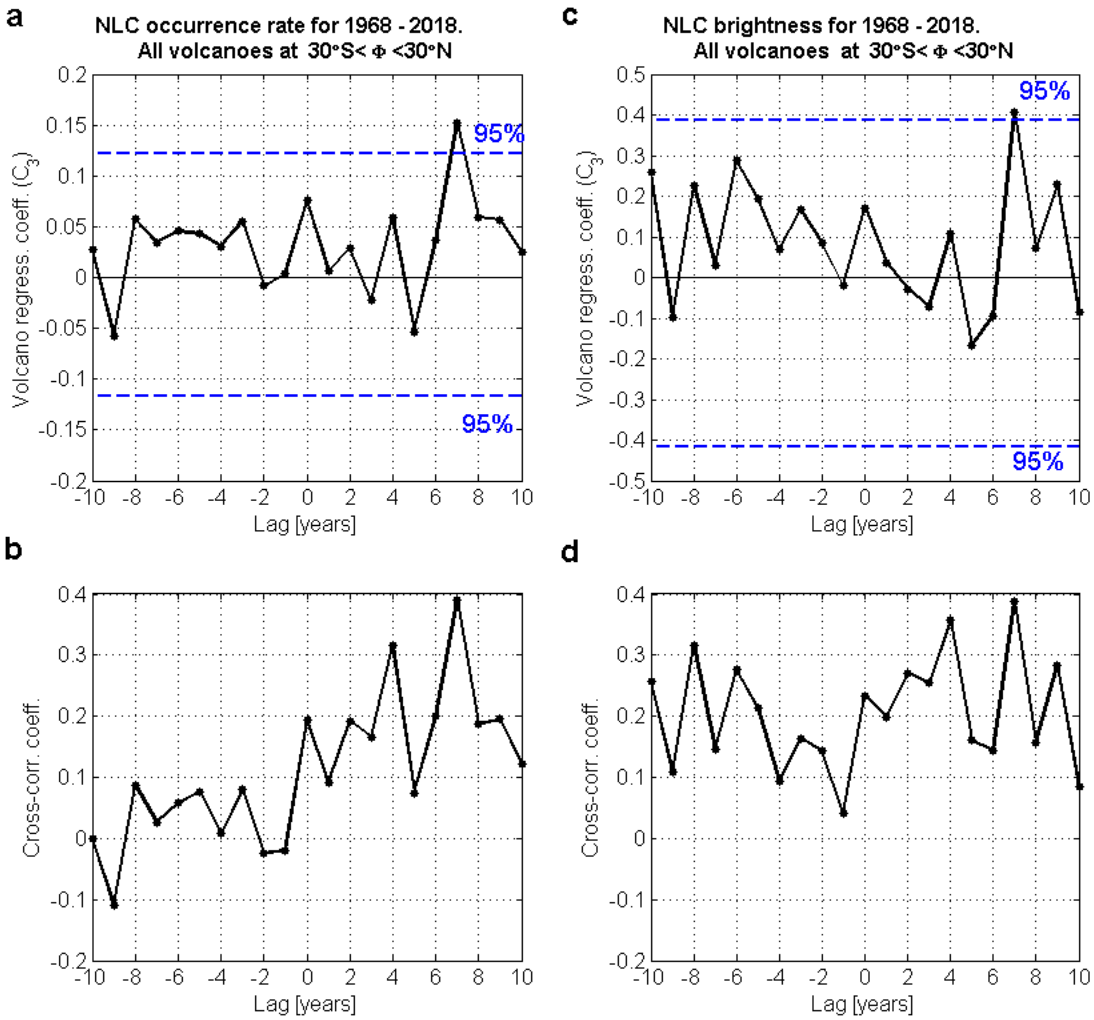

491
492

493 **Figure 4.** Statistical quantities characterizing a connection between volcanic and NLC
494 activity for all volcanic eruptions that occurred between 30°S and 30°N. **(a)** The back
495 line shows the volcanic regression coefficient (C_3) as a function of the phase time lag
496 for the NLC occurrence number. The blue lines indicate 95% confidence intervals of
497 the maximum value of the C_3 coefficient. **(b)** The cross-correlation coefficient is
498 between the NLC occurrence number and volcanic activity. **(c)** Same as in **(a)** except
499 for the NLC brightness. **(d)** Same as in **(b)** except for the NLC brightness.

500

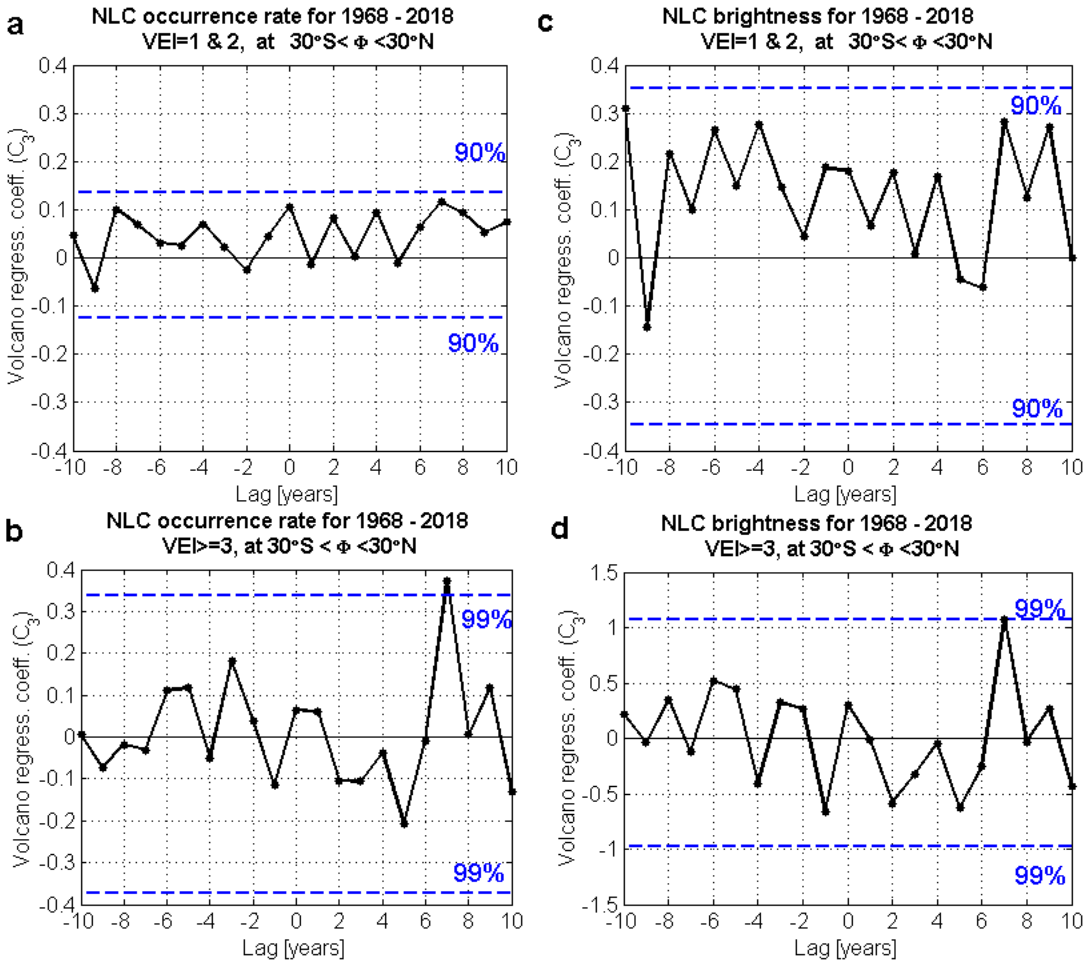

Figure 5. Statistical quantities characterizing a connection between volcanic and NLC activity for small, moderate and large volcanic eruptions that occurred between 30°S and 30°N. **(a)** The black line shows the volcanic regression coefficient (C_3) for the NLC occurrence number as a function of the phase time lag. The blue lines indicate confidence intervals of the maximum value of the C_3 coefficient. Results for minor volcanic eruptions, having VEI values equal to 1 and 2 marks, are shown. **(b)** Same as in **(a)** for moderate and large volcanic eruptions, having VEI values equal to 3 and more points. **(c)** Same as in **(a)** except for the NLC brightness. **(d)** Same as in **(b)** except for the NLC brightness.

Figure Legends

Figure 1. Overview of the analyzed data sets. **(a)** Volcanic activity data are represented by a sum of VEI values for each year from 1968 to 2018. Note that the two main eruptions in the time period considered (El Chichón in 1982 and Pinatubo in 1991) do not show up in the annually accumulated VEI values. **(b)** Annual NLC activity for the period of 1968-2018 is represented by the annual NLC occurrence number (black line with dots, left Y axis) and by the annual NLC brightness (red line with open circles, right Y axis).

Figure 2. Satellite measurements of volcanic SO_2 emissions. **(a)** The black dots are eruptive altitudes of SO_2 emissions as a function of VEI values. The red dots are SO_2 mean altitudes for the respective VEI values. The blue line is a linear function of mean SO_2 altitudes fitted in the least-square sense. **(b)** Same as in **(a)** except for the mass of ejected SO_2 emissions. Note that the X axis represents a logarithmic scale of the volcanic activity (VEI values). Linear regression functions are statistically significant with probabilities of 96% **(a)** and 88% **(b)**.

Figure 3. Statistical quantities characterizing a connection between volcanic and NLC activity for all volcanic eruptions that occurred around the world. **(a)** The black line shows the volcanic regression coefficient (C_3) as a function of the phase time lag for the NLC occurrence number. The blue lines indicate 90% confidence intervals of the maximum value of the C_3 coefficient. **(b)** The back line shows the cross-correlation coefficient between the NLC occurrence number and volcanic activity. The red line represents the cross-correlation coefficient between the NLC occurrence number and solar Lyman α flux. **(c)** Same as in **(a)** except for the NLC brightness. **(d)** The black line shows the cross-correlation coefficient between the NLC brightness and volcanic activity.

Figure 4. Statistical quantities characterizing a connection between volcanic and NLC activity for all volcanic eruptions that occurred between 30°S and 30°N. **(a)** The back line shows the volcanic regression coefficient (C_3) as a function of the phase time lag for the NLC occurrence number. The blue lines indicate 95% confidence intervals of the maximum value of the C_3 coefficient. **(b)** The cross-correlation coefficient is

between the NLC occurrence number and volcanic activity. **(c)** Same as in **(a)** except for the NLC brightness. **(d)** Same as in **(b)** except for the NLC brightness.

Figure 5. Statistical quantities characterizing a connection between volcanic and NLC activity for small, moderate and large volcanic eruptions that occurred between 30°S and 30°N. **(a)** The black line shows the volcanic regression coefficient (C_3) for the NLC occurrence number as a function of the phase time lag. The blue lines indicate confidence intervals of the maximum value of the C_3 coefficient. Results for minor volcanic eruptions, having VEI values equal to 1 and 2 marks, are shown. **(b)** Same as in **(a)** for moderate and large volcanic eruptions, having VEI values equal to 3 and more points. **(c)** Same as in **(a)** except for the NLC brightness. **(d)** Same as in **(b)** except for the NLC brightness.

Table 1. Regression coefficients of the multiple regression model (see equation 1), along with their standard deviations (1.5 or 2 or 3 standard deviations) for the NLC occurrence number and NLC brightness for the period of 1968-2018. Corresponding confidence probabilities (90% or 95% or 99%) are shown in brackets. Statistically significant coefficients (equal to or greater than its error) at the corresponding confidence levels are marked in bold. The time regression coefficient (C_1) is expressed in value per year (V/yr), the solar regression coefficient (C_2) is expressed in value per solar flux unit (SFU, 10^{11} photons cm^{-2} s^{-1}), the volcanic regression coefficient (C_3) is expressed in value per VEI (Value/VEI), C_0 is the regression constant. Phase lags (years) are introduced for the Lyman α flux and VEI. The P values for the null hypothesis test have been calculated for each regression coefficient. Table 1 represents three model runs with three different selections of volcanic activity:

a) all volcanic eruptions that occurred around the world (all VEI values, all longitudes and all latitudes);

b) volcanic eruptions with all VEI values at all longitudes and at latitudes between 30°S and 30°N;

c) volcanic eruptions with VEI>=3 at all longitudes and at latitudes between 30°S and 30°N.

(a) All volcanic eruptions (all VEI, all longitudes and all latitudes)				
	C_0 (V)	C_1 (V/yr)	C_2 (V/SFU) and lag (yr)	C_3 (V/VEI) and lag (yr)
NLC occurrence number	**40.0±14.1** (99%), P=0.0	-0.003±0.087 (90%), P=0.960	**-2.066±1.831** (95%), lag=0, P=0.028	**0.105±0.083** (90%), lag=7, P=0.038
NLC brightness	**111.1±44.3** (99%), P=0.0	0.159±0.272 (90%), P=0.330	**-8.599±7.673** (99%), lag=0, P=0.004	**0.305±0.259** (90%), lag=7, P=0.054
(b) Volcanoes with all VEI, all longitudes and latitudes between 30°S and 30°N				
NLC occurrence number	**41.8±12.6** (99%), P=0.0	-0.027±0.089 (90%), P=0.619	**-2.145±1.793** (95%), lag=0, P=0.020	**0.152±0.122** (95%), lag=7, P=0.016
NLC brightness	**117.3±39.9** (99%), P=0.0	0.102±0.284 (90%), P=0.549	**-8.832±7.615** (99%), lag=0, P=0.003	**0.406±0.387** (95%), lag=7, P=0.040
(c) Volcanoes with VEI>=3, all longitudes and latitudes between 30°S and 30°N				
NLC occurrence number	**44.7±11.5** (99%), P=0.0	-0.021±0.084 (90%), P=0.674	**-2.359±2.345** (99%), lag=0, P=0.010	**0.373±0.339** (99%), lag=7, P=0.005
NLC brightness	**124.8±36.4** (99%), P=0.0	0.106±0.267 (90%), P=0.506	**-9.442±7.409** (99%), lag=0, P=0.001	**1.070±1.071** (99%), lag=7, P=0.010

Figure 1.

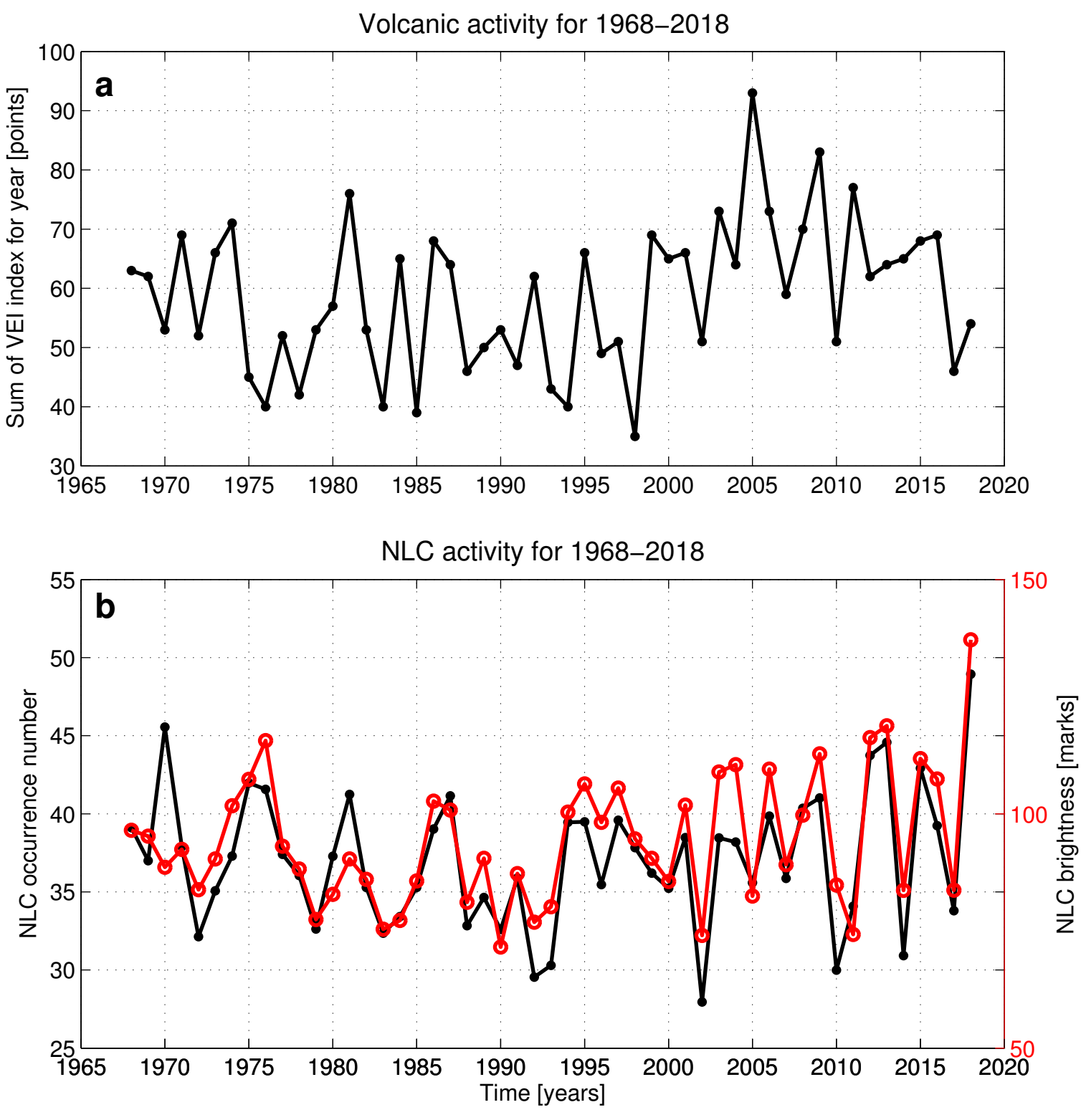
Volcanic activity for 1968–2018
a
Sum of VEI index for year [points]
100
90
80
70
60
50
40
30
1965
1970
1975
1980
1985
1990
1995
2000
2005
2010
2015
2020
NLC activity for 1968–2018
b
NLC occurrence number
NLC brightness [marks]
55
50
45
40
35
30
25
150
100
50
Time [years]

Figure 2.

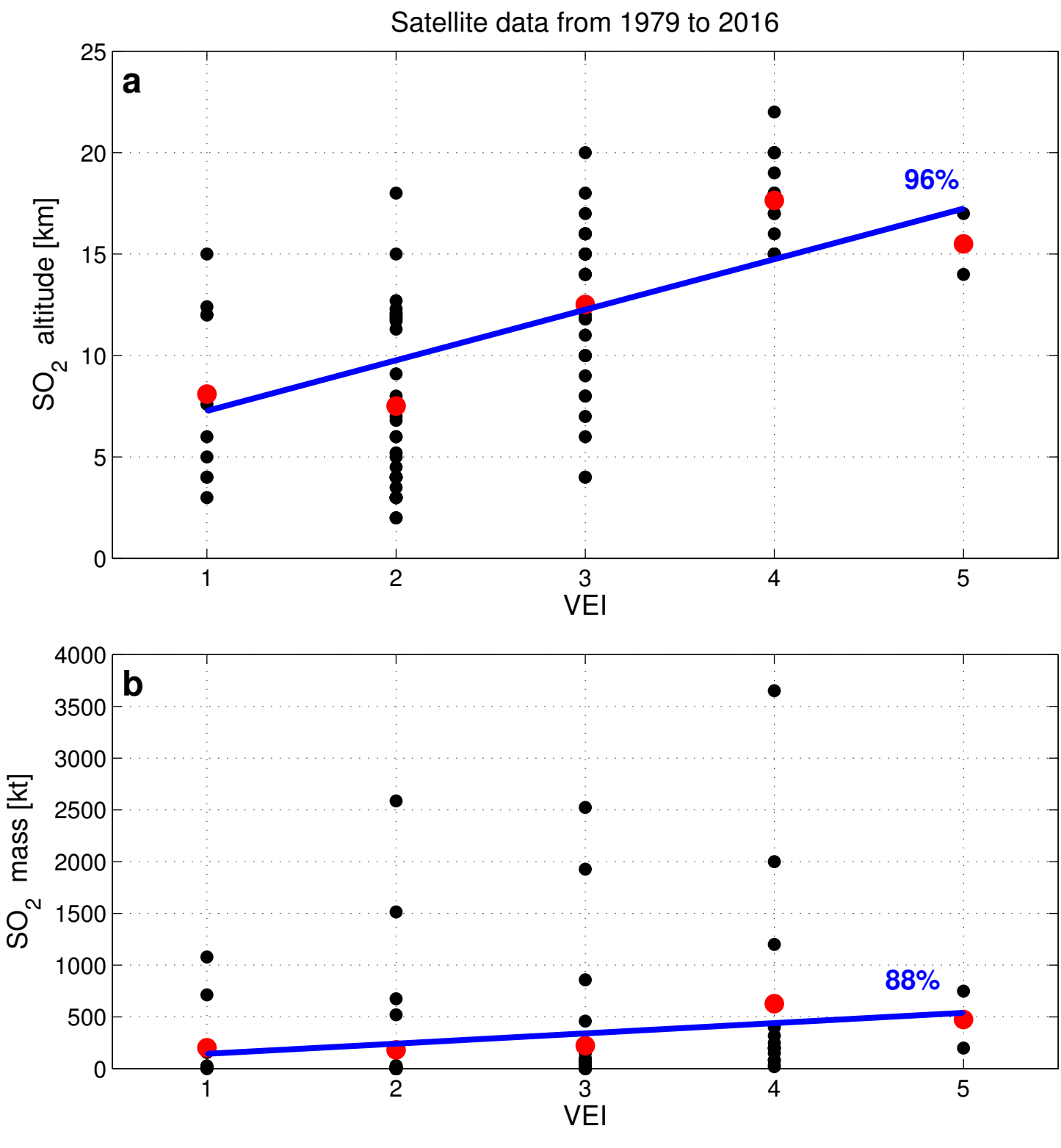
Satellite data from 1979 to 2016
a
96%
SO2 altitude [km]
VEI
b
88%
SO2 mass [kt]
VEI

Figure 3.

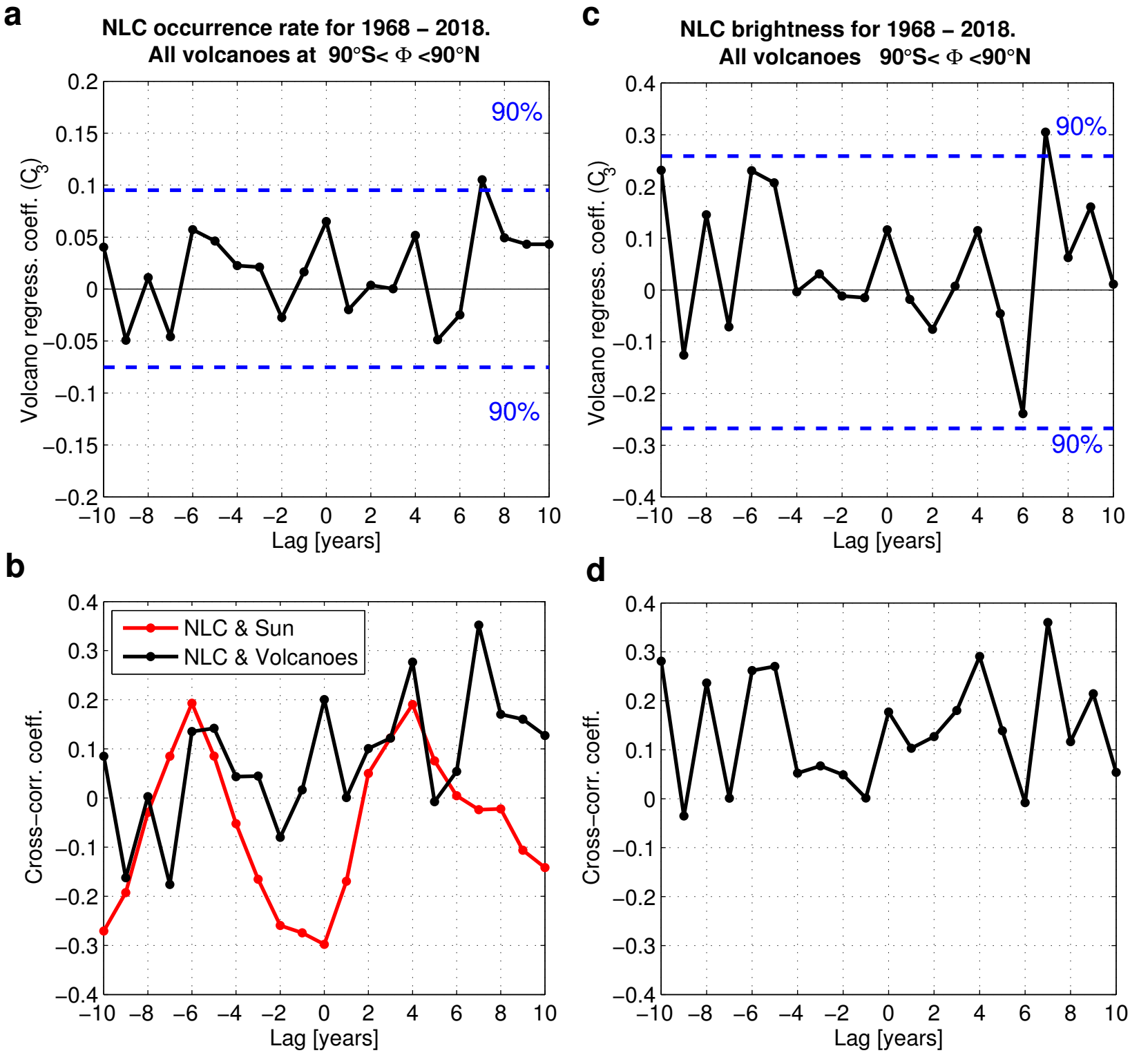
a
NLC occurrence rate for 1968 – 2018.
All volcanoes at 90°S< Φ <90°N
90%
90%
Volcano regress. coeff. (C3)
Lag [years]
c
NLC brightness for 1968 – 2018.
All volcanoes 90°S< Φ <90°N
90%
90%
Volcano regress. coeff. (C3)
Lag [years]
b
NLC & Sun
NLC & Volcanoes
Cross–corr. coeff.
Lag [years]
d
Cross–corr. coeff.
Lag [years]

Figure 4.

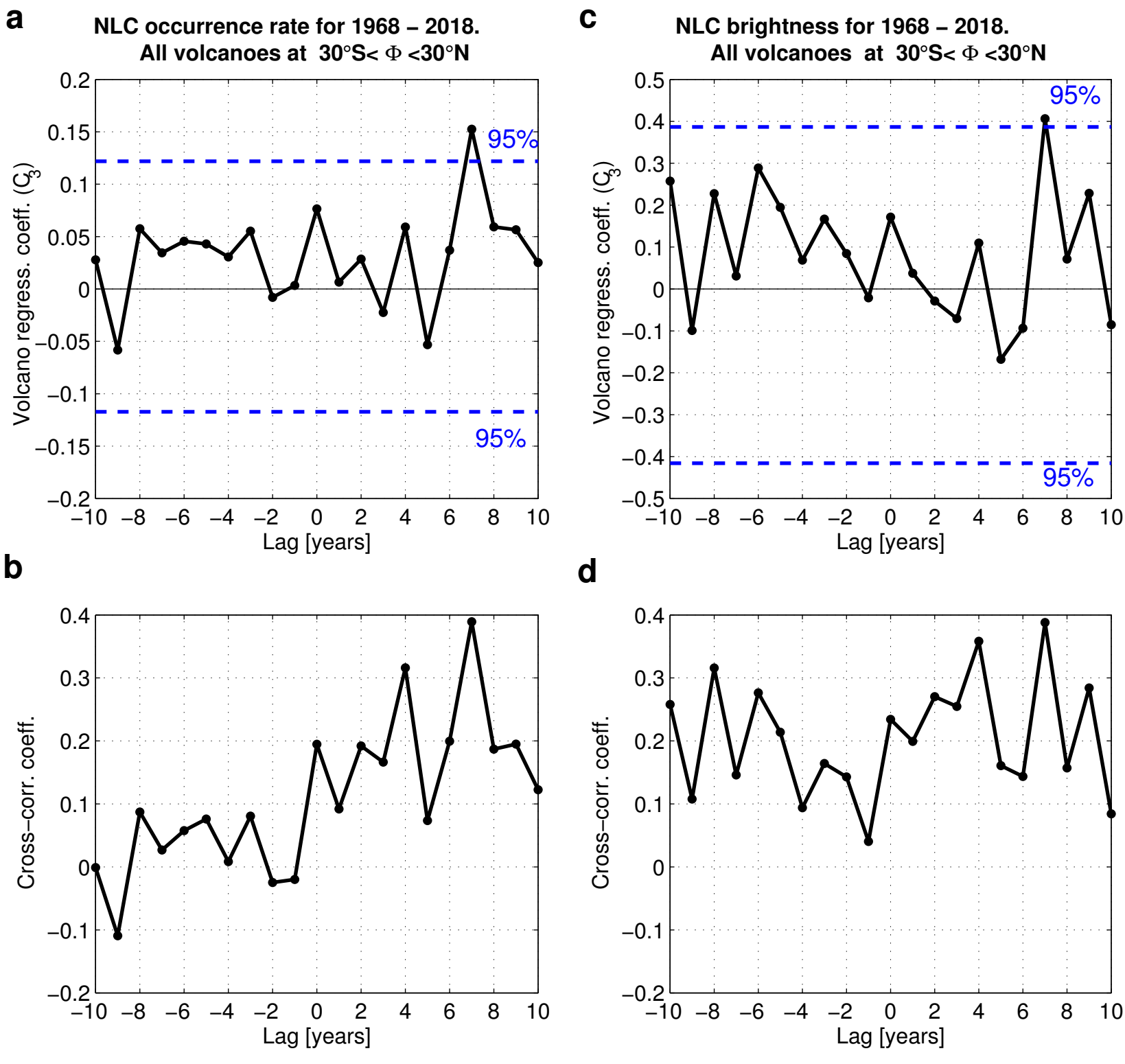
a
NLC occurrence rate for 1968 – 2018.
All volcanoes at 30°S< Φ <30°N
Volcano regress. coeff. (C3)
95%
95%
Lag [years]
c
NLC brightness for 1968 – 2018.
All volcanoes at 30°S< Φ <30°N
Volcano regress. coeff. (C3)
95%
95%
Lag [years]
b
Cross–corr. coeff.
Lag [years]
d
Cross–corr. coeff.
Lag [years]

Figure 5.

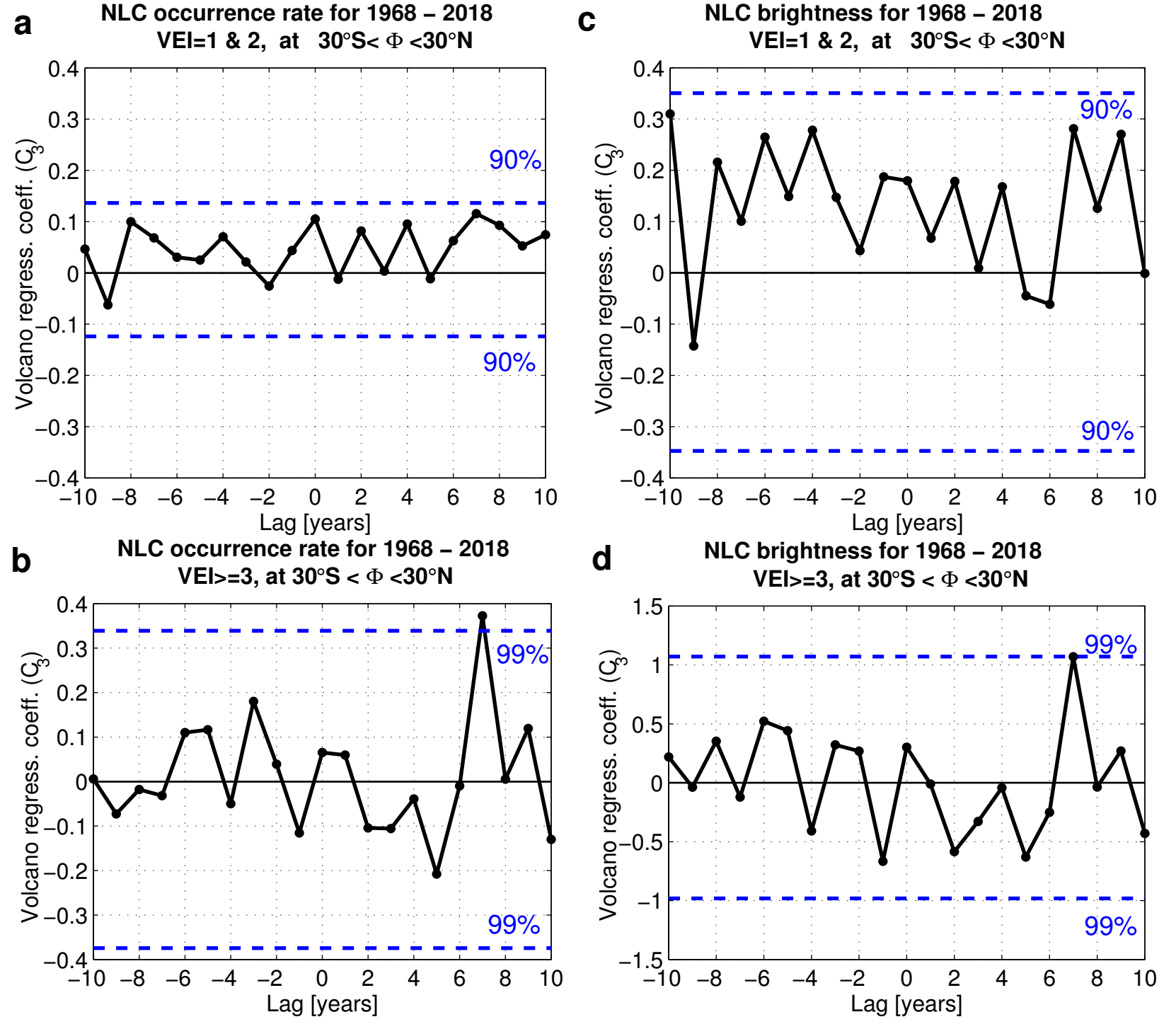
a
NLC occurrence rate for 1968 – 2018
VEI=1 & 2, at 30°S< Φ <30°N
Volcano regress. coeff. (C3)
Lag [years]
90%
90%
b
NLC occurrence rate for 1968 – 2018
VEI>=3, at 30°S < Φ <30°N
Volcano regress. coeff. (C3)
Lag [years]
99%
99%
c
NLC brightness for 1968 – 2018
VEI=1 & 2, at 30°S< Φ <30°N
Volcano regress. coeff. (C3)
Lag [years]
90%
90%
d
NLC brightness for 1968 – 2018
VEI>=3, at 30°S < Φ <30°N
Volcano regress. coeff. (C3)
Lag [years]
99%
99%

Table 1. Regression coefficients of the multiple regression model (see equation 1), along with their standard deviations (1.5 or 2 or 3 standard deviations) for the NLC occurrence number and NLC brightness for the period of 1968-2018. Corresponding confidence probabilities (90% or 95% or 99%) are shown in brackets. Statistically significant coefficients (equal to or greater than its error) at the corresponding confidence levels are marked in bold. The time regression coefficient (C_1) is expressed in value per year (V/yr), the solar regression coefficient (C_2) is expressed in value per solar flux unit (SFU, 10^{11} photons cm^{-2} s^{-1}), the volcanic regression coefficient (C_3) is expressed in value per VEI (Value/VEI), C_0 is the regression constant. Phase lags (years) are introduced for the Lyman α flux and VEI. The P values for the null hypothesis test have been calculated for each regression coefficient. Table 1 represents three model runs with three different selections of volcanic activity:

a) all volcanic eruptions that occurred around the world (all VEI values, all longitudes and all latitudes);

b) volcanic eruptions with all VEI values at all longitudes and at latitudes between 30°S and 30°N;

c) volcanic eruptions with VEI>=3 at all longitudes and at latitudes between 30°S and 30°N.

(a) All volcanic eruptions (all VEI, all longitudes and all latitudes)				
	C_0 (V)	C_1 (V/yr)	C_2 (V/SFU) and lag (yr)	C_3 (V/VEI) and lag (yr)
NLC occurrence number	**40.0±14.1** (99%), P=0.0	-0.003±0.087 (90%), P=0.960	**-2.066±1.831** (95%), lag=0, P=0.028	**0.105±0.083** (90%), lag=7, P=0.038
NLC brightness	**111.1±44.3** (99%), P=0.0	0.159±0.272 (90%), P=0.330	**-8.599±7.673** (99%), lag=0, P=0.004	**0.305±0.259** (90%), lag=7, P=0.054
(b) Volcanoes with all VEI, all longitudes and latitudes between 30°S and 30°N				
NLC occurrence number	**41.8±12.6** (99%), P=0.0	-0.027±0.089 (90%), P=0.619	**-2.145±1.793** (95%), lag=0, P=0.020	**0.152±0.122** (95%), lag=7, P=0.016
NLC brightness	**117.3±39.9** (99%), P=0.0	0.102±0.284 (90%), P=0.549	**-8.832±7.615** (99%), lag=0, P=0.003	**0.406±0.387** (95%), lag=7, P=0.040
(c) Volcanoes with VEI>=3, all longitudes and latitudes between 30°S and 30°N				
NLC occurrence number	**44.7±11.5** (99%), P=0.0	-0.021±0.084 (90%), P=0.674	**-2.359±2.345** (99%), lag=0, P=0.010	**0.373±0.339** (99%), lag=7, P=0.005
NLC brightness	**124.8±36.4** (99%), P=0.0	0.106±0.267 (90%), P=0.506	**-9.442±7.409** (99%), lag=0, P=0.001	**1.070±1.071** (99%), lag=7, P=0.010